Received: 30 March 2022 | Revised: 14 September 2022 | Accepted: 29 October 2022

DOI: 10.1002/dad2.12381

Alzheimer's & Dementia
Diagnosis, Assessment & Disease Monitoring

RESEARCH ARTICLE

Associations between diffusion MRI microstructure and cerebrospinal fluid markers of Alzheimer's disease pathology and neurodegeneration along the Alzheimer's disease continuum

Jason F. Moody[1] | **Douglas C. Dean III**[2,3,4] | **Steve R. Kecskemeti**[2] | **Kaj Blennow**[7,8] | **Henrik Zetterberg**[7,8,9,10,11] | **Gwendlyn Kollmorgen**[12] | **Ivonne Suridjan**[13] | **Norbert Wild**[12] | **Cynthia M. Carlsson**[1] | **Sterling C. Johnson**[1,6] | **Andrew L. Alexander**[2,3,5] | **Barbara B. Bendlin**[1]

[1]Wisconsin Alzheimer's Disease Research Center, University of Wisconsin-Madison, Madison, Wisconsin, USA

[2]Waisman Center, University of Wisconsin-Madison, Madison, Wisconsin, USA

[3]Department of Medical Physics, University of Wisconsin-Madison, Madison, Wisconsin, USA

[4]Department of Pediatrics, University of Wisconsin-Madison, Madison, Wisconsin, USA

[5]Department of Psychiatry, University of Wisconsin-Madison, Madison, Wisconsin, USA

[6]Geriatric Research Education and Clinical Center, Middleton Memorial VA Hospital, Madison, Wisconsin, USA

[7]Department of Psychiatry and Neurochemistry, Institute of Neuroscience and Physiology, Sahlgrenska Academy, University of Gothenburg, Mölndal, Sweden

[8]Clinical Neurochemistry Laboratory, Sahlgrenska University Hospital, Mölndal, Sweden

[9]Department of Neurodegenerative Disease, UCL Institute of Neurology, London, UK

[10]UK Dementia Research Institute, UCL, London, UK

[11]Hong Kong Center for Neurodegenerative Diseases, Hong Kong, China

[12]Roche Diagnostics GmbH, Penzberg, Germany

[13]Roche Diagnostics International Ltd, Rotkreuz, Switzerland

Correspondence
Jason F. Moody, Wisconsin Alzheimer's Disease Research Center, University of Wisconsin-Madison, 600 Highland Avenue J5/1M Clinical Science Center MC 2420, Madison, WI 53792, USA.
Email: jfmoody@wisc.edu

Abstract

Introduction: White matter (WM) degeneration is a critical component of early Alzheimer's disease (AD) pathophysiology. Diffusion-weighted imaging (DWI) models, including diffusion tensor imaging (DTI), neurite orientation dispersion and density imaging (NODDI), and mean apparent propagator MRI (MAP-MRI), have the potential to identify early neurodegenerative WM changes associated with AD.

Methods: We imaged 213 (198 cognitively unimpaired) aging adults with DWI and used tract-based spatial statistics to compare 15 DWI metrics of WM microstructure to 9 cerebrospinal fluid (CSF) markers of AD pathology and neurodegeneration treated as continuous variables.

Results: We found widespread WM injury in AD, as indexed by robust associations between DWI metrics and CSF biomarkers. MAP-MRI had more spatially diffuse relationships with $A\beta_{42/40}$ and pTau, compared with NODDI and DTI.

Discussion: Our results suggest that WM degeneration may be more pervasive in AD than is commonly appreciated and that innovative DWI models such as MAP-MRI may provide clinically viable biomarkers of AD-related neurodegeneration in the earliest stages of AD progression.

KEYWORDS
Alzheimer's disease, CSF biomarkers, diffusion MRI, DTI, early detection, MAP-MRI, Neuro, NODDI, preclinical, white matter microstructure

1 | INTRODUCTION

Degeneration of subcortical white matter (WM) is increasingly recognized as a critical process of early Alzheimer's disease (AD) pathophysiology, with some studies suggesting that WM degeneration may precede cortical atrophy.[1–5] Given that neurodegeneration is closely associated with cognitive dysfunction in AD, the discovery and development of reliable and sensitive in-vivo markers for neurodegeneration are important goals of AD research, as these prospective measures may aid in the identification of cognitively unimpaired individuals who are at risk for developing AD in the future, as well as provide crucial information pertaining to the staging and progression of AD.[6]

WM changes are commonly studied using diffusion-weighted imaging (DWI), a modality that operates by sensitizing the magnetic resonance imaging (MRI) signal to the diffusion of water molecules in the brain. The most prevalent DWI model used to study WM changes associated with AD is diffusion tensor imaging (DTI).[6] While DTI studies of AD have been informative, the model has known limitations, including providing limited information in regions with greater restricted (non-Gaussian) diffusion, such as that present within cellular structures.[7,8] An increasingly popular alternative to DTI applied in contemporary AD research is neurite orientation density and dispersion imaging (NODDI).[9] NODDI is a biophysically-based model which characterizes brain changes in specific microstructural environments by assuming that the DWI signal emanates from 3 distinct tissue compartments: within neurites, outside of neurites, and free water.[9] The primary NODDI measures are the neurite density index (NDI - the signal fraction from within neurites), the orientation dispersion index (ODI - the degree of angular variation among neurites), and the isotropic volume fraction (ISO – the signal fraction from a free water compartment). NODDI has shown promise for evaluating neurodegeneration along the clinical continuum of AD,[10–12] as well as alterations along the biological spectrum of AD pathology.[13]

An alternative DWI model with minimal assumptions about tissue microstructure is mean apparent propagator (MAP) MRI.[14,15] In MAP-MRI, the probability density function describing the displacements of diffusing water molecules is estimated directly from the DWI signal. MAP-MRI measures include the return to origin probability (RTOP), the return to axis probability (RTAP), the return to plane probability (RTPP), the mean squared displacement (MSD), the Non-Gaussianity (NG), and the q-space inverse variance (QIV).[14,15] RTOP quantifies the probability that a proton will remain in the same relative position in 3D space between 2 consecutive diffusion gradient pulses, and therefore, is a marker for tissue restriction. RTAP and RTPP are the 2D and 1D counterparts of RTOP and are sensitive to restrictive barriers perpendicular and parallel to the principal direction of diffusion, respectively. NG, which can similarly be decomposed into components that are perpendicular ($NG_{\perp}$) and parallel ($NG_{\parallel}$) to the principal direction of diffusion, represents the fraction of the DWI signal that does not conform to a Gaussian distribution, and therefore, serves as a barometer for complex tissue organization. MSD, another indicator of tissue restriction, is a measure of how far diffusing water molecules travel between successive diffusion gradient pulses. Finally, QIV is a measure of the variance in the diffusion signal.[14–16] Recently, MAP-MRI has been shown to be more useful than DTI for the evaluation of Parkinson's disease severity[17] as well as temporal lobe epilepsy lateralization.[18] Additionally, 1 study found evidence that MAP-MRI was sensitive to age-dependent amyloid burden in transgenic Alzheimer rats (TgF344-AD),[19] paving the way for future studies to explore the potential of MAP-MRI to identify AD-related microstructural changes in humans.

In order to investigate WM microstructural alterations associated with AD across the brain, we applied DTI, NODDI, and for the very first time, MAP-MRI to assess the relationships between 15 distinct diffusion parameters of WM microstructure and 9 cerebrospinal fluid (CSF) markers of AD pathology (amyloid-beta$_{42/40}$ ratio [$A\beta_{42/40}$] and phosphorylated tau [pTau]), axonal degeneration (neurofilament light chain [NfL])[20], synaptic degeneration (neurogranin,[21] α-synuclein[22]), and glial activation (glial fibrillary acidic protein [GFAP],[23] soluble triggering receptor expressed on myeloid cells 2 [sTREM2],[24] chitinase-3-like protein 1 [YKL-40][25]). Our goal was to utilize a broad assortment of DWI markers to determine the extent to which WM microstructure is affected along the AD continuum in a largely preclinical population.

TABLE 1 Participant demographics

N	213
Males, *n* (%)	78 (36.6)
Females, *n* (%)	135 (63.4)
Age in years, Mean (SD)	64.6 (7.3)
APOE ε4 carriers, *n* (% of sample)	70 (32.9)
CU/MCI/AD, *n*	198/13/2
CSF biomarker cutoff groups, *n* (% of sample):	
A+/T−, *n* (%)	19 (8.9)
A−/T+, *n* (%)	13 (6.1)
A−/T−, *n* (%)	164 (77.0)
A+/T+, *n* (%)	17 (8.0)

RESEARCH IN CONTEXT

1. **Systematic review**: We used PubMed to comprehensively review literature focused on diffusion-weighted imaging (DWI) studies of brain changes associated with Alzheimer's disease (AD). Numerous studies have used diffusion tensor imaging (DTI) to identify microstructural brain alterations associated with cerebrospinal fluid (CSF) markers of AD pathology and neurodegeneration. However, very few have used neurite orientation dispersion and density imaging (NODDI), and none have used mean apparent propagator (MAP) MRI. To our knowledge, this constitutes the first study of white matter (WM) changes associated with AD using MAP-MRI.
2. **Interpretation**: Our results suggest that WM alterations are more extensive in AD progression than is commonly appreciated and that sophisticated DWI models such as MAP-MRI may be better suited for detecting early AD-related neurodegeneration than conventional DTI.
3. **Future directions**: Studies which implement advanced DWI techniques such as MAP-MRI may provide invaluable biomarkers for the detection of incipient pathological brain changes associated with early AD.

2 | METHODS

2.1 | Participant selection

We identified 213 participants (Table 1) from the Wisconsin Alzheimer's Disease Research Center (ADRC, $n = 95$) and Wisconsin Registry for Alzheimer's Prevention study (WRAP, $n = 118$) who underwent both multi-shell DWI and lumbar puncture. Based on neuropsychological testing and clinical criteria established by the National Institute on Aging and Alzheimer's Association, each participant was given a clinical diagnosis of cognitively unimpaired (CU, $n = 198$), mild cognitive impairment due to AD (MCI, $n = 13$), or AD dementia (AD, $n = 2$). The average time between lumbar puncture and DWI scan across all participants was 142 days (median: 91, standard deviation [SD]: 125, range: 562). All study procedures were approved by The University of Wisconsin Health Sciences Institutional Review Board and all participants provided written informed consent.

2.2 | CSF biomarker acquisition and designation of amyloid and tau pathology status

CSF samples were collected via lumbar puncture after a minimum 4-hour fast, stored a −80°C, and assayed at the Clinical Neurochemistry Laboratory, University of Gothenburg with the Roche NeuroToolKit (NTK).[26] Immunoassays were performed on either a cobas e 601 analyzer (Elecsys β-Amyloid (1-42) CSF, β-Amyloid (1-40) CSF, Elecsys Phospho-Tau (181P) CSF) or a cobas e 411 analyzer (NfL, neurogranin, α-synuclein, GFAP, sTREM2, and YKL-40).

Cutoffs (+ or −) for amyloid ($A\beta_{42/40}$) and tau (pTau) pathologies were established as follows: the $A\beta_{42/40}$ threshold (<0.046, $A\beta_{42/40}$+) was derived using receiver operator characteristic (ROC) curve analysis in combination with Youden's J statistic, utilizing [C-11] Pittsburgh compound B positron emission tomography imaging positivity as the standard of comparison. The pTau threshold (≥ 24.8 pg/mL, pTau+) was designated to be 2 SD above the mean of a reference group of 223 $A\beta_{42/40}$− cognitively unimpaired younger participants whose age ranged between 45 and 60 years.[20,26]

2.3 | DWI acquisition and processing

Participants were scanned on 1 of 2 3T MR750 scanners (GE Healthcare, Waukesha, WI) with 32-channel head coils (Nova Medical; Wilmington, MA) located at either the Waisman Center ($n_{scanner1} = 59$) or the Wisconsin Institute for Medical Research at UW-Health ($n_{scanner2} = 154$), in Madison, WI. DWI images were acquired using either a 3-shell or 5-shell DWI protocol. DWI acquisition parameters are provided in Table S1.

All DWI images were corrected for noise,[27] Gibbs ringing,[27] and eddy current-induced distortions[28–30] and 5-shell images were corrected for susceptibility-induced distortions.[31] Diffusion tensors were estimated in each voxel with weighted least squares regression using b values <1500 s/mm^2 (i.e., the 2 inner shells) and DTI parameter maps (FA, MD, RD, AxD) were computed. The NODDI model was implemented via the Diffusion Microstructure Imaging in Python toolbox,[32] using $d_{\parallel} = 1.7$ μm2/ms, to calculate NDI, ODI, and ISO parameter maps. MAP-MRI was applied to the diffusion data with Diffusion Imaging in Python software,[33] which fit the DWI signal to Hermite basis functions using a radial order of 6 and regularized the corresponding basis coefficients with the Laplacian of the reconstructed signal.[16] The regularized

basis coefficients were utilized to calculate parameter maps of RTOP, RTAP, RTPP, MSD, NG, $NG_{\perp}$, $NG_{\parallel}$, and QIV (Figure S1).

2.4 | Tract-based spatial statistics (TBSS) processing

In order to evaluate the relationship between all diffusion metrics and CSF biomarkers across WM regions, diffusion parameter maps were processed with the TBSS pipeline.[34] FA maps for all 213 participants were registered to MNI 152 1 mm^3 space with nonlinear registration.[30] The resultant warps were used to register the other 14 diffusion parameter maps into the same space. The FA maps in MNI space were used to estimate a population mean FA (WM) skeleton via a cutoff FA value of 0.2, and all other DWI metrics were projected onto this skeleton so that statistical analysis could be performed.

2.5 | Data harmonization

Prior to statistical testing, all diffusion data were harmonized across scanner (scanner 1 vs. scanner 2) and diffusion protocol (3 shell vs. 5 shell) using neuroHarmonize software in Python.[35,36] NeuroHarmonize allows for the application of the Combat algorithm, a well-established technique that was first introduced to remove batch-effects in genomics,[37] directly to the harmonization of quantitative brain imaging data. Age and sex were specified as linear covariates, so that only the effects of scanner and diffusion protocol were minimized during the harmonization process.

2.6 | Linear modeling and statistics

Each imaging voxel was fit to the following general linear model (GLM) using *Randomise*[38]:

$$\text{DiffusionParamter} = \beta_0 + \beta_1 * (\text{CSFbiomarker}) + \beta_2 * (\text{Age}) + \beta_3 * (\text{sex}) + \varepsilon \quad (1)$$

This model is linear with respect to CSF biomarker (continuous variable) and incudes age (continuous variable) and sex (categorical variable) as covariates. All data were demeaned, and threshold-free cluster enhancement[39] was utilized to identify clusters of WM skeleton voxels that exhibited significant associations between diffusion parameters and CSF biomarkers after nonparametric permutation testing (with 5000 permutations), correcting for multiple comparisons across voxels ($P_{corr} < 0.05$). In order to preserve statistical power, no corrections for multiple comparisons were made across DWI-CSF associations.

The percentage of WM skeleton voxels exhibiting significant associations between diffusion parameters and CSF biomarkers were computed for each DWI-CSF marker pair along with corresponding effect sizes (Cohen's f2). Binary masks of these voxels were created and combined to: (1) count the number of diffusion parameters significantly associated with each of $A\beta_{42/42}$, pTau, pTau/$A\beta_{42}$, and NfL in each WM voxel and (2) compare the composite associations of MAP-MRI (combining associations of RTOP, RTAP, RTPP, MSD, NG, $NG_{\perp}$ $NG_{\parallel}$, QIV), NODDI (combining associations of NDI, ODI, ISO), and DTI (combining associations of FA, MD, RD, AxD) metrics to $A\beta_{42/42}$, pTau, pTau/$A\beta_{42}$, and NfL, respectively.

2.7 | Supplementary analyses

We performed 4 supplementary analyses: (1) To ascertain the relationship between diffusion metrics and CSF biomarkers of AD pathology in an entirely preclinical population, we excluded all MCI and AD participants from our analysis and ran the same GLM (Equation 1) in the 198 cognitively unimpaired controls in our sample. (2) To increase the sensitivity of DTI metrics to CSF biomarkers, we recomputed DTI maps utilizing an additional shell of DWI data (up to $b = 2000$ s/mm^2 in the 3-shell dataset and up to $b = 2700$ s/mm^2 in the 5-shell dataset) and reran the GLM (Equation 1) with these alternative DTI maps. (3) To test the effectiveness of the data harmonization across diffusion protocols, we reran the GLM (Equation 1) with the 3-shell ($n = 153$) and 5-shell ($n = 60$) diffusion parameter maps independently and compared the number and direction (+ or −) of resultant significant relationships. (4) To gauge the strength of associations across different WM regions in the brain, we extracted DWI metrics from 3 WM ROIs (the corpus callosum [CC], cingulum [CING], and superior longitudinal fasciculus [SLF]) using the JHU ICBM WM atlas[40] and computed partial Pearson correlations between select DWI measures and CSF markers, correcting for age and sex.

3 | RESULTS

3.1 | Widespread associations with markers of AD pathology and axonal degeneration

Overall, there were widespread significant relationships between diffusion metrics of WM microstructure and CSF markers for amyloid plaques, phosphorylated tau proteins, and axonal degeneration across the brain (Figures 1–3, Table 2). CSF NfL, an indicator of axonal degeneration, was significantly associated with 9 different diffusion parameters (Positive: ODI, ISO, MSD, QIV; Negative: NDI, RTPP, NG, NG, $NG_{\perp}$), pTau/$A\beta_{42}$ was associated with 7 parameters (Positive: ODI, QIV; Negative: NDI, RTPP, NG, $NG_{\perp}$, $NG_{\parallel}$), pTau with 6 (Positive: ODI, QIV; Negative: NDI, RTPP, NG, $NG_{\perp}$), and $A\beta_{42/40}$ was positively associated with 4 (NDI, RTOP, NG, and $NG_{\perp}$). Three different diffusion metrics, NG, $NG_{\perp}$, and NDI, were each significantly associated with $A\beta_{42/40}$, pTau, pTau/$A\beta_{42}$, and NfL. Of note, $NG_{\perp}$ had the most extensive association with any of the 9 CSF markers among the 15 diffusion parameters assessed. Notably, 91.5% of the WM skeleton exhibited a significant relationship between $NG_{\perp}$ and pTau. Meanwhile,

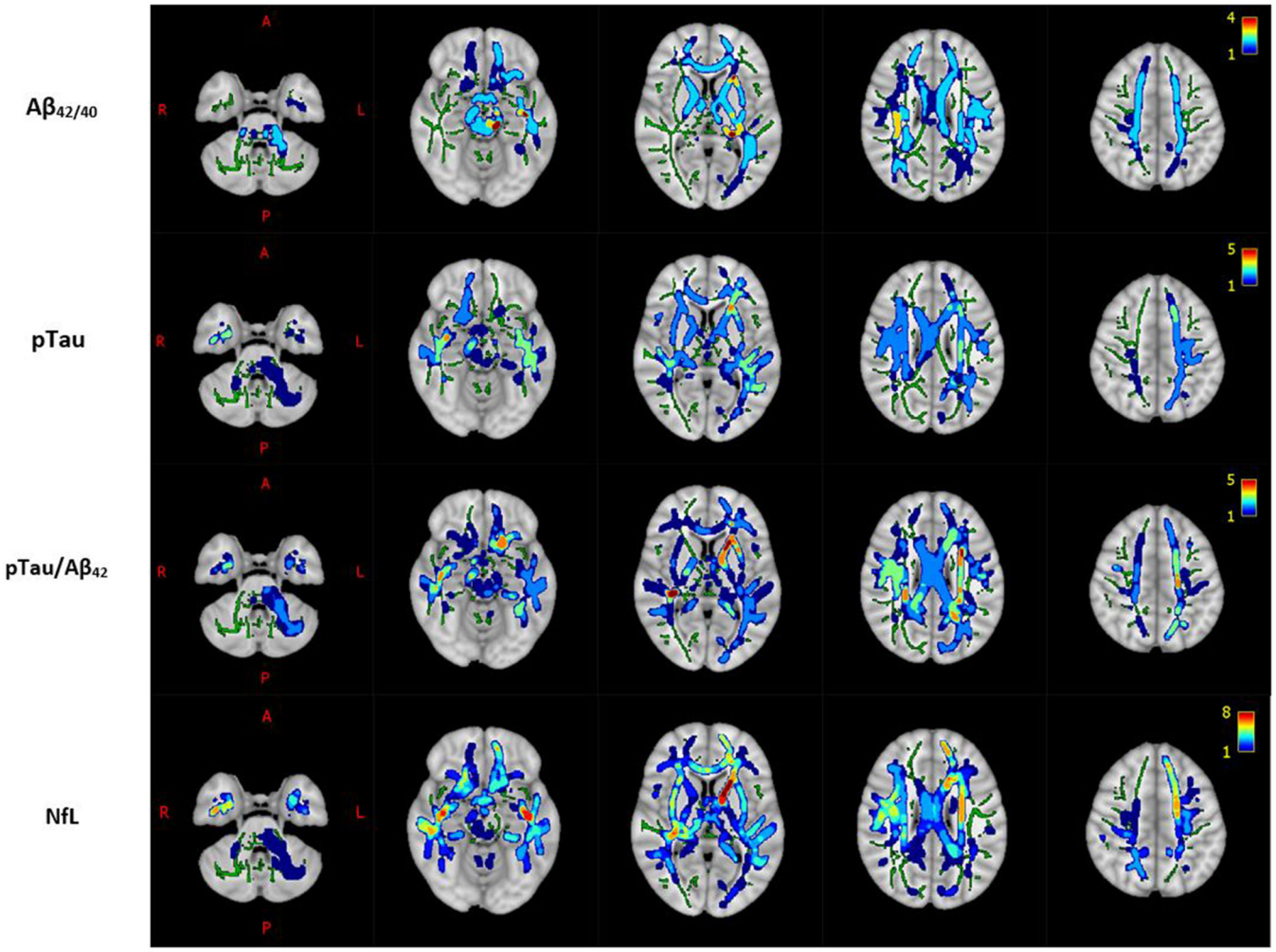

FIGURE 1 Count of diffusion parameters having significant associations with CSF markers of AD pathology and neurodegeneration overlaid on the 1 mm MNI 152 standard T1 template. Each voxel is color-coded by the number of diffusion parameters that have significant associations with the given CSF marker (top row: $A\beta_{42/40}$, 2nd row: pTau, 3rd row: pTau/AB42, bottom row: NfL) in that voxel. WM is delineated by the mean FA skeleton of all subjects (green). Results are corrected for age, sex, and multiple comparisons across voxels with $p < 0.05$.

TABLE 2 Percentage of WM skeleton voxels with significant associations (positive: bold, negative: light, or none: blank) between CSF markers and diffusion parameters of WM microstructure (corrected for age, sex, and multiple comparisons across voxels, $p < 0.05$) in 213 participants

CSF Marker	FA	MD	RD	AxD	NDI	ODI	ISO	RTOP	RTAP	RTPP	MSD	NG	$NG_{\perp}$	$NG_{\parallel}$	QIV
$A\beta_{42}/A\beta_{40}$					**49.0**			**70.6**				**26.3**	**25.8**		
pTau					3.0	**3.0**				8.0		82.2	91.5		**30.9**
pTau/$A\beta_{42}$					84.2	**10.3**				3.3		25.0	14.2	41.7	**62.1**
NfL					77.4	**24.7**	**57.8**			80.6	**3.7**	59.0	41.7	14.0	**83.1**
α-synuclein												7.6	35.5		
sTREM2		**31.7**	**7.6**	**10.7**								2.8	49.6		
GFAP	**0.53**				**60.6**		9.5				26.5				
Neurogranin															
YKL-40															

Note: That the associations between each DWI-CSF marker pair were always in the same direction across WM voxels.

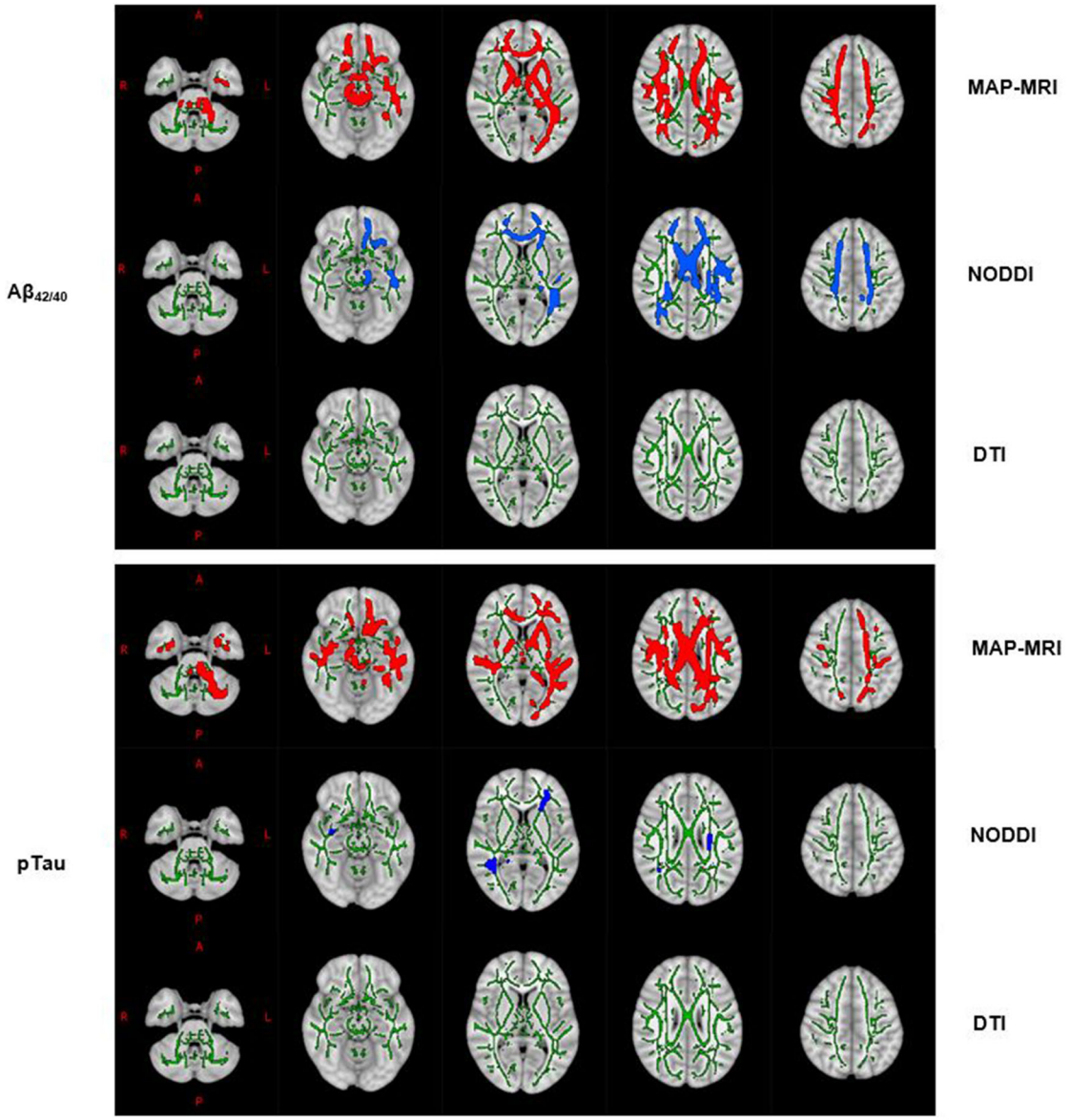

FIGURE 2 WM skeleton voxels (highlighted using the TBSS_fill command) with significant associations between CSF markers (top panel: $A\beta_{42/40}$, bottom panel: pTau) and DWI Metrics (MAP-MRI: Red, NODDI: Blue, DTI: None) overlaid on the 1 mm MNI 152 standard T1 template. WM is delineated by the mean FA skeleton of all subjects (green). Results are corrected for age, sex, and multiple comparisons across voxels with $p < 0.05$.

NG was also extensively related to pTau in 82.2% of WM skeleton voxels, while NDI was pervasively associated with pTau/$A\beta_{42}$ in 84.2% of WM skeleton voxels. Of the 9 total associations between diffusion microstructural parameters and NfL, QIV and RTPP were the most prevalent, with 83.1% and 80.6% of WM skeleton voxels related for each metric, respectively (Table 2). Most of the significant DWI-CSF relationships persisted in separate analyses of the 3-shell and 5-shell data (Tables S5–S6) and 21 different DWI-CSF marker pairs exhibited significant associations when analysis was restricted to 198 preclinical participants (Table S3).

When the 2 inner shells of DWI data were used to fit diffusion tensors to each imaging voxel (all b values <1500 s/mm^2), no DTI metrics had significant relationships with $A\beta_{42/40}$, pTau, pTau/ $A\beta_{42}$, or NfL that survived corrections for age, sex, and multiple comparisons across voxels (Table 2). However, when incorporating an extra shell into the DTI model, RD, MD, and AxD were all positively associated with NfL, while MD and RD were positively related to pTau/$A\beta_{42}$ (Table S4).

WM regions with the largest number of total diffusion parameters associated with CSF markers included the CING, CC, and SLF (Figure 1). Conversely, areas with the fewest number were primarily concentrated in the brainstem and peripheral brain regions. Partial correlations between select CSF markers and DWI metrics extracted from the CC, CING, and SLF ranged from weak to moderate (Figures S2–S5).

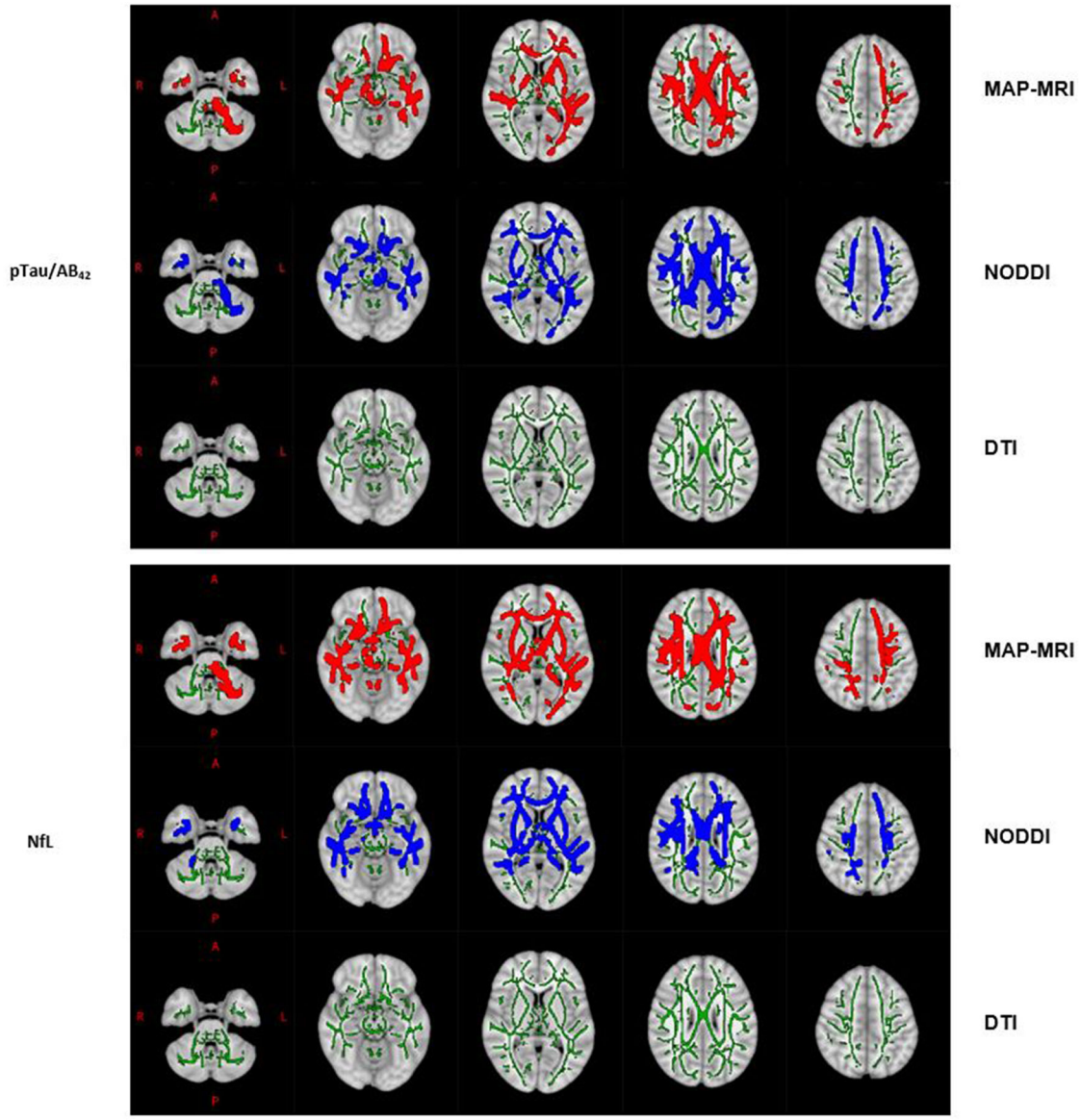

FIGURE 3 WM skeleton voxels (highlighted using the TBSS_fill command) with significant associations between CSF markers (top panel: pTau/Aβ_{42}, bottom panel: NfL) and DWI metrics (MAP-MRI: rbed, NODDI: blue, DTI: none) overlaid on the 1 mm MNI 152 standard T1 template. WM is delineated by the mean FA skeleton of all subjects (green). Results are corrected for age, sex, and multiple comparisons across voxels with $p < 0.05$.

3.2 | MAP-MRI and sensitivity to amyloid and tau pathology

A comparison of DWI techniques revealed that MAP-MRI metrics had particularly widespread associations with A$\beta_{42/40}$ and pTau and larger corresponding effect sizes, compared with NODDI and DTI metrics (Figure 2, Table 2, Table S2). With respect to A$\beta_{42/40}$, 3 of the 4 diffusion indices that had significant associations with this amyloid biomarker were MAP-MRI metrics (RTOP, NG, and NG$_\perp$), with RTOP being the most prevalent. Comparably, of the 6-diffusion metrics meaningfully related to pTau, 4 were MAP-MRI metrics (RTPP, NG, NG$_\perp$, QIV), with NG$_\perp$ having the most robust relationship to pTau (Table 2). Despite differing sensitivities to A$\beta_{42/40}$ and pTau levels, MAP-MRI and NODDI performed similarly in being able to detect changes in pTau/Aβ_{42} across the brain (Figure 3).

3.3 | Associations with markers of synaptic degeneration, glial activation, and inflammation

Notable associations between DWI metrics and sTREM2, GFAP, and α-synuclein were also observed. There were 5 diffusion metrics with a meaningful relationship to sTREM2 (Positive: MD, RD, AxD; Negative: NG, NG$_\perp$), 4 to GFAP (Positive: FA, NDI; Negative: ISO, MSD), and 2 to α-synuclein (Negative: NG, NG$_\perp$). These included particularly large associations between NG$_\perp$ and α-synuclein (in 35.5% of WM skeleton

voxels) and sTREM2 (in 49.6% of WM skeleton voxels) as well as between NDI and GFAP (in 60.6% of WM skeleton voxels). Lastly, there were zero significant associations between any diffusion parameter and YKL-40 or neurogranin (Table 2).

4 | DISCUSSION

While MRI investigations of neurodegeneration in AD have most commonly focused on gross macrostructural brain changes, such as reduced cortical volume and thickness, there is now considerable evidence to suggest that neurodegeneration can be captured with techniques sensitive to tissue microstructure along the AD continuum even prior to cortical atrophy.[13] Furthermore, studies have shown that degenerative WM microstructural changes, including axonal degeneration, demyelination, inflammation, and alterations in cellularity, are involved in AD and methods that measure these phenomena provide useful and complementary information related to the onset and progression of AD pathology. In this study, we used 3 distinct DWI techniques to identify widespread relationships between CSF markers of AD and DWI markers of WM degeneration along the AD continuum, which may suggest that little subcortical WM is spared from the effects of AD.

4.1 | DWI is a clinically viable tool for identifying microstructural changes associated with AD

The widespread sensitivity of DWI microstructural metrics to CSF biomarkers of AD pathology and neurodegeneration suggests that DWI may have untapped potential in a clinical setting. For example, among our participants, NDI, NG, and $NG_{|}$ each had associations with at least 4 different CSF markers that covered more than 20% of the WM skeleton. The extensive associations between diffusion parameters and CSF biomarkers of AD pathology in a largely preclinical sample such as ours, suggests that these measures may hold the potential to identify the very earliest WM microstructural alterations associated with AD in cognitively unimpaired adults, years before the manifestation of cognitive and clinical symptoms of dementia. Correspondingly, after removing MCI and AD participants from our sample, over 20 associations between DWI metrics and CSF markers remained significant, including 6 diffusion metrics that were sensitive to NfL (NDI, ODI, ISO, RTPP, NG, $NG_{\perp}$), 4 to pTau/Aβ_{42} (NDI, ODI, RTOP, $NG_{\parallel}$), 4 to A$\beta_{42/40}$ (NDI, RTOP, NG, $NG_{\perp}$), and 3 to pTau (NG, $NG_{\perp}$). While the associations were much less extensive across the WM skeleton voxels of the brain, there remained 8 different DWI indices that had some significant sensitivity to CSF markers of AD pathology or neurodegeneration, among our preclinical cohort. Notably, the diffusion imaging sequences applied in this study can be acquired in under 10 min,[42] making the derivation of these metrics a clinically viable tool for early detection of AD-related neurodegeneration.

4.2 | MAP-MRI and NODDI may be sensitive to microstructural signatures of AD-related neurodegeneration

In our study, MAP-MRI outperformed NODDI and DTI in detecting changes in CSF biomarkers of AD pathology and neurodegeneration across the WM fiber bundles of the brain. This may be a consequence of the fact that MAP-MRI metrics more directly relate to the microstructural features of brain tissue and characterize non-Gaussian diffusion profiles indicative of more complex tissue organization. Therefore, these markers may be especially sensitive to common neurodegenerative changes, including those central to AD pathology, such as axonal degeneration, demyelination, inflammation, and reductions in tissue cellularity.

For example, water diffusion is highly restricted within axons, dendrites, and cellular membranes and organelles, resulting in non-Gaussian diffusion. Decreased Non-Gaussianity (NG) from MAP-MRI suggests reduced tissue complexity and is likely a sensitive marker of axonal loss and demyelination,[15] which are 2 hallmark features of AD-related WM degeneration.[43,44] NfL, which was predictive of NG, $NG_{\perp}$, and $NG_{\parallel}$ in our sample, is sensitive to both.[45,46] Moreover, $NG_{\perp}$ had a strikingly widespread association with α-synuclein, a presynaptic protein and known marker for synaptic degeneration.[22] In this context, it is likely that damaged synapses (in the cortices) are concurrently affecting nearby (subcortical) WM and that $NG_{\perp}$, by detecting subtle increases in diffusion Gaussianity in the affected area, is sensitive to this damage. Additionally, higher A$\beta_{42/40}$ levels in our sample were predictive of widespread increases in RTOP, suggesting that amyloid accumulation in AD is associated with pervasive reductions in tissue restriction.

Furthermore, MAP-MRI and NODDI metrics exhibited widespread associations with pTau/Aβ_{42}, and NfL. Notably, increases in both markers were predictive of extensive reductions in NDI, suggesting that reduced neurite density may be a characteristic feature of early AD pathology. These relationships pervaded association, commissural, projection and brainstem fiber bundles, spanning every lobule of the brain. While several studies of WM hyperintensities in AD have focused on frontal and temporal regions associated with memory and executive function,[47–49] our results suggest that WM changes in early pre-symptomatic stagers of AD progression might be more widespread than is commonly appreciated. It is possible that the microstructural WM changes detected by DWI indices in this study are happening on a whole brain scale, in parallel with well-documented global atrophy of WM and gray matter structures.

4.3 | Limitations

A few limitations should be noted. First, we are limited by our cross-sectional study design. Ideally, we would have multiple CSF biomarker measurements and DWIs per participant, so that we could better account for individual variability in brain structure and age-related

changes to both CSF and DWI markers. Second, some caution should be used when interpreting DWI indices and CSF biomarkers. For example, a change in RTOP may be dictated by changes in cellularity, myelination, and axonal volume.[14,15,50,51] Without corroborating histological studies, it can be difficult to attribute specific DWI measurements to specific tissue properties. Similarly, in a mostly preclinical cohort, pTau does not directly reflect the regional accumulation of neurofibrillary tangles and is probably, at least in part, indicative of a neuronal response to the deposition of β-amyloid proteins.[13,52] As a result, it is likely that some of our DWI associations with pTau are artificially inflated by underlying amyloid pathology. Third, we did not consider the presence of WM hyperintensities (WMH) in our analysis. Because previous studies have shown that DTI[53] and NODDI[54] metrics are associated with the presence of WMH and because the majority of individuals over the age of 60 exhibit WMH,[53] we cannot rule out the possibility that some of our results may be influenced by uneven macrostructural WM damage between participants. Last, while data harmonization reduces the variability between DWI protocols, it cannot entirely remove protocol-dependent differences in sensitivity to tissue properties. Because of this, we assessed the associations between DWI metrics and CSF markers in the 3-shell and 5-shell cohorts independently, finding evidence that some of these relationships appear to be robust to differences in acquisition parameters.

ACKNOWLEDGMENTS

First and foremost, we thank the research participants at the UW ADRC and WRAP for their commitment and willingness to participate in this study. We also thank the research staff at the UW ADRC for their assistance in study organization, participant recruitment, facilitating data availability, and technical support. The Roche NTK is a panel of robust prototype biomarker assays designed to evaluate key pathologic events characteristic of AD and other neurological disorders, used for research purposes only and not approved for clinical use. ELECSYS and COBAS are trademarks of Roche. All other trademarks are property of their respective owners. This research was supported by Roche Diagnostics International Ltd (Rotkreuz, Switzerland), NIH grants R01AG037639 (to BBB), R01AG027161 (to SCJ), P30 AG062715, P50 HD105353 (Waisman Center Core Grant), and the Geriatric Research, Education, and Clinical Center of the William S. Middleton Memorial Veterans Hospital. JFM was supported by the National Institute of General Medical Sciences (NIH/NIGMS) - Initiative for Maximizing Student Development (IMSD – Grant No. R25 GM083252), the Biology of Aging and Age-Related Diseases Training Grant (Grant No. T32 AG000213), and the SciMed Graduate Research Scholars Fellowship. HZ is a Wallenberg Scholar supported by grants from the Swedish Research Council (#2018-02532), the European Research Council (#681712), Swedish State Support for Clinical Research (#ALFGBG-720931), the Alzheimer Drug Discovery Foundation (ADDF), USA (#201809-2016862), the AD Strategic Fund and the Alzheimer's Association (#ADSF-21-831376-C, #ADSF-21-831381-C and #ADSF-21-831377-C), the Olav Thon Foundation, the Erling-Persson Family Foundation, Stiftelsen för Gamla Tjänarinnor, Hjärnfonden, Sweden (#FO2019-0228), the European Union's Horizon 2020 research and innovation programme under the Marie Skłodowska-Curie grant agreement No 860197 (MIRIADE), European Union Joint Program for Neurodegenerative Disorders (JPND2021-00694), and the UK Dementia Research Institute at UCL. KB is supported by the Swedish Research Council (#2017-00915), the Alzheimer Drug Discovery Foundation (ADDF), USA (#RDAPB-201809-2016615), the Swedish Alzheimer Foundation (#AF-930351, #AF-939721 and #AF-968270), Hjärnfonden, Sweden (#FO2017-0243 and #ALZ2022-0006), the Swedish state under the agreement between the Swedish government and the County Councils, the ALF-agreement (#ALFGBG-715986 and #ALFGBG-965240), the European Union Joint Program for Neurodegenerative Disorders (JPND2019-466-236), the National Institute of Health (NIH), USA, (grant #1R01AG068398-01), and the Alzheimer's Association 2021 Zenith Award (ZEN-21-848495).

CONFLICT OF INTEREST

H.Z. has served at scientific advisory boards and/or as a consultant for Abbvie, Alector, Annexon, Artery Therapeutics, AZTherapies, CogRx, Denali, Eisai, Nervgen, Novo Nordisk, Pinteon Therapeutics, Red Abbey Labs, Passage Bio, Roche, Samumed, Siemens Healthineers, Triplet Therapeutics, and Wave, has given lectures in symposia sponsored by Cellectricon, Fujirebio, Alzecure, Biogen, and Roche, and is a co-founder of Brain Biomarker Solutions in Gothenburg AB (BBS), which is a part of the GU Ventures Incubator Program (outside submitted work). K.B. has served as a consultant, at advisory boards, or at data monitoring committees for Abcam, Axon, BioArctic, Biogen, JOMDD/Shimadzu. Julius Clinical, Lilly, MagQu, Novartis, Ono Pharma, Pharmatrophix, Prothena, Roche Diagnostics, and Siemens Healthineers, and is a co-founder of Brain Biomarker Solutions in Gothenburg AB (BBS), which is a part of the GU Ventures Incubator Program, outside the work presented in this paper. All other authors have no competing interests to disclose. Author disclosures are available in the supporting information.

REFERENCES

1. Agosta F, Pievani M, Sala S, et al. White matter damage in Alzheimer disease and its relationship to gray matter atrophy. *Radiology*. 2011;258(3):853-863. doi:10.1148/radiol.10101284
2. Canu E, McLaren DG, Fitzgerald ME, et al. Microstructural diffusion changes are independent of macrostructural volume loss in moderate to severe Alzheimer's disease. *J Alzheimers Dis*. 2010;19(3):963-976. doi:10.3233/JAD-2010-1295
3. Maier-Hein KH, Westin CF, Shenton ME, et al. Widespread white matter degeneration preceding the onset of dementia. *Alzheimers Dement*. 2015;11(5):485-493.e2. doi:10.1016/j.jalz.2014.04.518
4. Salat DH, Tuch DS, van der Kouwe AJW, et al. White matter pathology isolates the hippocampal formation in Alzheimer's disease. *Neurobiol Aging*. 2010;31(2):244-256. doi:10.1016/j.neurobiolaging.2008.03.013
5. Stricker NH, Salat DH, Foley JM, et al. Decreased white matter integrity in neuropsychologically defined mild cognitive impairment is independent of cortical thinning. *J Int Neuropsychol Soc*. 2013;19(8):925-937. doi:10.1017/S1355617713000660

6. Alm KH, Bakker A. Relationships between diffusion tensor imaging and cerebrospinal fluid metrics in early stages of the Alzheimer's disease continuum. *J Alzheimers Dis*. 2019;70(4):965-981. doi:10.3233/JAD-181210
7. Jones DK, Knösche TR, Turner R. White matter integrity, fiber count, and other fallacies: the do's and don'ts of diffusion MRI. *Neuroimage*. 2013;73:239-254. doi:10.1016/j.neuroimage.2012.06.081
8. Alexander AL, Lee JE, Lazar M, Field AS. Diffusion tensor imaging of the brain. *Neurotherapeutics*. 2007;4(3):316-329. doi:10.1016/j.nurt.2007.05.011
9. Zhang H, Schneider T, Wheeler-Kingshott CA, Alexander DC. NODDI: practical in vivo neurite orientation dispersion and density imaging of the human brain. *NeuroImage*. 2012;61(4):1000-1016. doi:10.1016/j.neuroimage.2012.03.072
10. Vogt NM, Hunt JF, Adluru N, et al. Cortical microstructural alterations in mild cognitive impairment and Alzheimer's disease dementia. *Cerebral Cortex*. 2020;30(5):2948-2960. doi:10.1093/cercor/bhz286
11. Parker TD, Slattery CF, Zhang J, et al. Cortical microstructure in young onset Alzheimer's disease using neurite orientation dispersion and density imaging. *Hum Brain Mapp*. 2018;39(7):3005-3017. doi:10.1002/hbm.24056
12. Fu X, Shrestha S, Sun M, et al. Microstructural white matter alterations in mild cognitive impairment and Alzheimer's disease. *Clin Neuroradiol*. 2020;30(3):569-579. doi:10.1007/s00062-019-00805-0
13. Vogt NM, Hunt JFV, Adluru N, et al. Interaction of amyloid and tau on cortical microstructure in cognitively unimpaired adults. *Alzheimers Dement*. 2022;18(1):65-76. doi:10.1002/alz.12364
14. Özarslan E, Koay CG, Shepherd TM, et al. Mean apparent propagator (MAP) MRI: a novel diffusion imaging method for mapping tissue microstructure. *Neuroimage*. 2013;78:16-32. doi:10.1016/j.neuroimage.2013.04.016
15. Avram AV, Sarlls JE, Barnett AS, et al. Clinical feasibility of using mean apparent propagator (MAP) MRI to characterize brain tissue microstructure. *NeuroImage*. 2016;127:422-434. doi:10.1016/j.neuroimage.2015.11.027
16. Fick RHJ, Wassermann D, Caruyer E, Deriche R. MAPL: tissue microstructure estimation using Laplacian-regularized MAP-MRI and its application to HCP data. *Neuroimage*. 2016;134:365-385. doi:10.1016/j.neuroimage.2016.03.046
17. Le H, Zeng W, Zhang H, et al. Mean apparent propagator MRI is better than conventional diffusion tensor imaging for the evaluation of Parkinson's disease: a prospective pilot study. *Front Aging Neurosci*. 2020;12:306. doi:10.3389/fnagi.2020.563595
18. Ma K, Zhang X, Zhang H, et al. Mean apparent propagator-MRI: a new diffusion model which improves temporal lobe epilepsy lateralization. *Eur J Radiol*. 2020;126:108914. doi:10.1016/j.ejrad.2020.108914
19. Fick RHJ, Daianu M, Pizzolato M. Comparison of biomarkers in transgenic Alzheimer rats using multi-shell diffusion MRI. In: Fuster A, Ghosh A, Kaden E, Rathi Y, Reisert M, eds. *Computational Diffusion MRI*. Mathematics and Visualization. Springer International Publishing; 2017:187-199. doi:10.1007/978-3-319-54130-3_16
20. Ian XiongY, T Meng, Luo J, ZhangH The potential of neurofilament light as a biomarker in Alzheimer's disease. *ENE*. 2021;84(1):6-15. doi:10.1159/000513008
21. Casaletto KB, Elahi FM, Bettcher BM, et al. Neurogranin, a synaptic protein, is associated with memory independent of Alzheimer biomarkers. *Neurology*. 2017;89(17):1782-1788. doi:10.1212/WNL.0000000000004569
22. Twohig D, Nielsen HM. α-synuclein in the pathophysiology of Alzheimer's disease. *Mol Neurodegener*. 2019;14(1):23. doi:10.1186/s13024-019-0320-x
23. Teitsdottir UD, Jonsdottir MK, Lund SH, Darreh-Shori T, Snaedal J, Petersen PH. Association of glial and neuronal degeneration markers with Alzheimer's disease cerebrospinal fluid profile and cognitive functions. *Alzheimers Res Ther*. 2020;12(1):92. doi:10.1186/s13195-020-00657-8
24. Rauchmann BS, Sadlon A, Perneczky R. Alzheimer's disease neuroimaging initiative. Soluble TREM2 and inflammatory proteins in Alzheimer's disease cerebrospinal fluid. *J Alzheimers Dis*. 2020;73(4):1615-1626. doi:10.3233/JAD-191120
25. Craig-Schapiro R, Perrin RJ, Roe CM, et al. YKL-40: a novel prognostic fluid biomarker for preclinical Alzheimer's disease. *Biol Psychiatry*. 2010;68(10):903-912. doi:10.1016/j.biopsych.2010.08.025
26. Van Hulle C, Jonaitis EM, Betthauser TJ, et al. An examination of a novel multipanel of CSF biomarkers in the Alzheimer's disease clinical and pathological continuum. *Alzheimers Dement*. 2021;17(3):431-445. doi:10.1002/alz.12204
27. Tournier JD, Smith R, Raffelt D, et al. MRtrix3: a fast, flexible and open software framework for medical image processing and visualisation. *NeuroImage*. 2019;202:116137. doi:10.1016/j.neuroimage.2019.116137
28. Andersson JLR, Sotiropoulos SN. An integrated approach to correction for off-resonance effects and subject movement in diffusion MR imaging. *Neuroimage*. 2016;125:1063-1078. doi:10.1016/j.neuroimage.2015.10.019
29. Andersson JLR, Graham MS, Zsoldos E, Sotiropoulos SN. Incorporating outlier detection and replacement into a non-parametric framework for movement and distortion correction of diffusion MR images. *Neuroimage*. 2016;141:556-572. doi:10.1016/j.neuroimage.2016.06.058
30. Jenkinson M, Beckmann CF, Behrens TEJ, Woolrich MW, Smith SMFSL. FSL. *Neuroimage*. 2012;62(2):782-790. doi:10.1016/j.neuroimage.2011.09.015
31. Andersson JLR, Skare S, Ashburner J. How to correct susceptibility distortions in spin-echo echo-planar images: application to diffusion tensor imaging. *Neuroimage*. 2003;20(2):870-888. doi:10.1016/S1053-8119(03)00336-7
32. Fick RHJ, Wassermann D, Deriche R. The dmipy toolbox: diffusion MRI multi-compartment modeling and microstructure recovery made easy. *Front Neuroinform*. 2019;13:64. doi:10.3389/fninf.2019.00064
33. Garyfallidis E, Brett M, Amirbekian B, et al. Dipy, a library for the analysis of diffusion MRI data. *Front Neuroinform*. 2014;8:8. doi:10.3389/fninf.2014.00008
34. Smith SM, Jenkinson M, Johansen-Berg H, et al. Tract-based spatial statistics: voxelwise analysis of multi-subject diffusion data. *Neuroimage*. 2006;31(4):1487-1505. doi:10.1016/j.neuroimage.2006.02.024
35. Fortin JP, Cullen N, Sheline YI, et al. Harmonization of cortical thickness measurements across scanners and sites. *NeuroImage*. 2018;167:104-120. doi:10.1016/j.neuroimage.2017.11.024
36. Pomponio R, Erus G, Habes M, et al. Harmonization of large MRI datasets for the analysis of brain imaging patterns throughout the lifespan. *NeuroImage*. 2020;208:116450. doi:10.1016/j.neuroimage.2019.116450
37. Johnson WE, Li C, Rabinovic A. Adjusting batch effects in microarray expression data using empirical Bayes methods. *Biostatistics*. 2007;8(1):118-127. doi:10.1093/biostatistics/kxj037
38. Winkler AM, Ridgway GR, Webster MA, Smith SM, Nichols TE. Permutation inference for the general linear model. *Neuroimage*. 2014;92:381-397. doi:10.1016/j.neuroimage.2014.01.060
39. Smith S, Nichols T. Threshold-free cluster enhancement: addressing problems of smoothing, threshold dependence and localisation in cluster inference. *NeuroImage*. 2009;44(1):83-98. doi:10.1016/j.neuroimage.2008.03.061
40. Fonov V, Evans AC, Botteron K, Almli CR, McKinstry RC, Collins DL. Unbiased average age-appropriate atlases for pediatric studies. *Neuroimage*. 2011;54(1):313-327. doi:10.1016/j.neuroimage.2010.07.033

41. Wang Q, Wang Y, Liu J, et al. Quantification of white matter cellularity and damage in preclinical and early symptomatic Alzheimer's disease. *Neuroimage Clin*. 2019;22:101767. doi:10.1016/j.nicl.2019.101767
42. Wu YC, Alexander AL. Hybrid diffusion imaging. *Neuroimage*. 2007;36(3):617-629. doi:10.1016/j.neuroimage.2007.02.050
43. Nasrabady SE, Rizvi B, Goldman JE, Brickman AM. White matter changes in Alzheimer's disease: a focus on myelin and oligodendrocytes. *Acta Neuropathol Commun*. 2018;6:22. doi:10.1186/s40478-018-0515-3
44. Papuć E, Rejdak K. The role of myelin damage in Alzheimer's disease pathology. *Arch Med Sci*. 2018;16(2):345-351. doi:10.5114/aoms.2018.76863
45. Bozzetti S, Ferrari S, Gajofatto A, Mariotto S. Neurofilament light chain in demyelinating conditions of the central nervous system: a promising biomarker. *Neuroimmunol Neuroinflammation*. 2021;8(1):1-13. 10.20517/2347-8659.2020.26
46. Weinhofer I, Rommer P, Zierfuss B, et al. Neurofilament light chain as a potential biomarker for monitoring neurodegeneration in X-linked adrenoleukodystrophy. *Nat Commun*. 2021;12(1):1816. doi:10.1038/s41467-021-22114-2
47. Parks CM, Iosif AM, Farias S, Reed B, Mungas D, DeCarli C. Executive function mediates effects of white matter hyperintensities on episodic memory. *Neuropsychologia*. 2011;49(10):2817-2824. doi:10.1016/j.neuropsychologia.2011.06.003
48. Mayo CD, Garcia-Barrera MA, Mazerolle EL, et al. Relationship between DTI metrics and cognitive function in Alzheimer's disease. *Front Aging Neurosci*. 2019;10:436. doi:10.3389/fnagi.2018.00436
49. Rizvi B, Lao PJ, Colón J, et al. Tract-defined regional white matter hyperintensities and memory. *Neuroimage Clin*. 2020;25:102143. doi:10.1016/j.nicl.2019.102143
50. Wu YC, Field AS, Whalen PJ, Alexander AL. Age- and gender-related changes in the normal human brain using hybrid diffusion imaging (HYDI). *Neuroimage*. 2011;54(3):1840-1853. doi:10.1016/j.neuroimage.2010.09.067
51. Fick RHJ, Pizzolato M, Wassermann D, Zucchelli M, Menegaz G, Deriche R. A sensitivity analysis of q-space indices with respect to changes in axonal diameter, dispersion and tissue composition. 2016:1241-1244. doi:10.1109/ISBI.2016.7493491
52. Calvo-Flores Guzmán B, Elizabeth Chaffey T, Hansika Palpagama T, et al. The interplay between beta-amyloid 1-42 (Aβ1-42)-induced hippocampal inflammatory response, p-tau, vascular pathology, and their synergistic contributions to neuronal death and behavioral deficits. *Front Mol Neurosci*. 2020;13:196. doi:10.3389/fnmol.2020.552073
53. Svärd D, Nilsson M, Lampinen B, et al. The effect of white matter hyperintensities on statistical analysis of diffusion tensor imaging in cognitively healthy elderly and prodromal Alzheimer's disease. *PLoS One*. 2017;12(9):e0185239. doi:10.1371/journal.pone.0185239
54. Raghavan S, Reid RI, Przybelski SA, et al. Diffusion models reveal white matter microstructural changes with ageing, pathology and cognition. *Brain Commun*. 2021;3(2). doi:10.1093/braincomms/fcab106

SUPPORTING INFORMATION

Additional supporting information can be found online in the Supporting Information section at the end of this article.

How to cite this article: Moody JF, Dean DC, Kecskemeti SR, et al. Associations between diffusion MRI microstructure and cerebrospinal fluid markers of Alzheimer's disease pathology and neurodegeneration along the Alzheimer's disease continuum. *Alzheimer's Dement*. 2022;14:e12381. https://doi.org/10.1002/dad2.12381